Discover Environment

Research

Chemical analyses and geographical origins of residential attic dust in central South Africa

Deidré van der Westhuizen[1] · Megan Welman-Purchase[2] · Janine Wichmann[3] · Karel G. von Eschwege[1]

Received: 2 September 2024 / Accepted: 2 April 2025
Published online: 10 April 2025

Abstract
Particulate matter (PM) is a widely used air pollution proxy indicator. Substantial supporting evidence links exposure to PM with adverse health effects. This study compares long-term accumulated particulate matter's chemical and morphological properties and possible sources from various locations in Bloemfontein, Kimberley, and the Vanderbijlpark residential areas. As the first study of this kind in South Africa, dust samples were collected from the attics of houses built over fifty years ago. Potential area PM sources located far away were identified by analyzing every tenth year from 1972 to 2022, representing five decades of backward Long-Range Transport (LRT) clusters, for air masses that passed the sampling sites. Several PM sources were determined by combining LRT geographic origin studies and chemical analyses of collected samples. Elemental compositions of samples were determined by the use of scanning electron microscopy, and electron dispersive spectroscopy. Mineral content was determined by X-ray fluorescence, X-ray diffraction, and electron probe microscopy techniques, revealing airborne sources that moved significantly due to climate change, over the 5-decade period. Potential area PM sources located far away included various South African provinces, neighboring states to the north, and the Atlantic and Indian Oceans west and east of South Africa. Elemental composition included: Al, Ag, C, Ca, Cl, Cu, Fe, K, Mg, Mn, Na, O, S, Si, Ti, and Zn. Mineral composition included SiO_2, TiO_2, Al_2O_3, Fe_2O_3, MnO, MgO, CaO, Na_2O, K_2O, P_2O_5, SO_3, Cr_2O_3 and NiO. The most prominent minerals found were quarts and plagioclase. While considering relevant mining activities, combining methods allowed a successful study of change in source distribution associated with climate change.

Keywords Air pollution · Dust particles · Trace elements · Minerals

1 Introduction

Globally, the number of premature deaths due to exposure to long-term air pollution is increasing every year and therefore became a matter of profound concern [1, 2]. Apart from causing ill health in many, pollution also drives climate change, and thus the consequent international outcry in favor of alternative green and sustainable technologies [3].

Supplementary Information The online version contains supplementary material available at https://doi.org/10.1007/s44274-025-00241-7.

✉ Karel G. von Eschwege, vEschwKG@ufs.ac.za; Deidré van der Westhuizen, didivdwesthuizen@gmail.com; Megan Welman-Purchase, purchasemd@ufs.ac.za; Janine Wichmann, janine.wichmann@up.ac.za | [1]Department of Chemistry, University of the Free State, PO Box 339, Bloemfontein 9300, South Africa. [2]Department of Geology, University of the Free State, PO Box 339, Bloemfontein 9300, South Africa. [3]School of Health Systems and Public Health, Faculty of Health Sciences, University of Pretoria, Pretoria, South Africa.

Particulate matter is but one part of air pollution in general, albeit a major component [2]. These particles include suspended particulate matter, inhalable larger PM_{10} particles (diameter of 10 µm or less), finer $PM_{2.5}$ particles (diameter of 2.5 µm or less), and ultrafine particles with a diameter of 100 nm or less. Long-term dust may include several of these categories, which may be the consequence of soil, environmental media, and meteorological conditions both at the location and far away, in the period over which it settled, as well as specific activities whereby it was generated [4]. Globally, the number of research reports addressing atmospheric particulate matter is increasing but tends to focus mostly on PM_{10} and $PM_{2.5}$. Previous studies in South Africa identified PM sources such as biomass burning, road traffic, and the agricultural and industrial sectors, but limited information is available on PM resulting from mining activities [5–9], which thus necessitates more research in related PM pollution.

A study done in Maribor, Slovenia, found mining sediments consisting of rock fragments containing garnet, epidote, zircon, quartz, etc. [10–12]. The mountains surrounding Maribor contain minerals to which the origin of the sampled dust could be ascribed [13–15]. Another study in Slovenia determined that airborne PM/dust entering attics is not influenced by indoor activities or weather conditions and therefore persistently accumulates over long periods of many years or even decades [16]. PM deposits in snow, urban soil, attics, streets, and residential dust were analyzed to determine particulate characteristics and chemical composition of the dust. In the Indrija area, many soil and attic dust samples were collected to study the effect of 500 years of mining. Mercury levels in the soil were found to exceed critical values for soil, while attic dust yielded Hg levels 3.6 times higher than this [17]. Similar analyses in lead-polluted mining areas showed man-made associations that resulted from lead and iron production in the vicinities [18, 19]. Pb-smelting was identified as a major source of pollution close to these industries. An attic dust study in Hungary revealed pollutants which included several toxic heavy metals, from both anthropogenic and background processes [20]. The authors concluded attic dust analyses to be an efficient and inexpensive method to assess long-term airborne contamination that may be associated with human health risks.

PM may often travel over long periods and even long distances and thus formally became known as long-range transport (LRT) clusters. A key tool used to determine the origin of these clusters is Backward Trajectory Modelling.

This study aimed to investigate the elemental and mineral composition and possibly local and distant sources of attic dust in residential areas at various central South African locations, namely in Bloemfontein, Kimberley, and Vanderbijlpark. Samples were collected from several houses in each of these cities, with PM sources identified every ten years over 50 years.

2 Materials and methods

2.1 Sampling

Dust in the attics of houses with tiled roofs was collected at 9 different sites in the three towns/cities, chosen for their proximity to main roads, infrastructure, and industry. Tiled roof covering provides ample openings between tiles for fine dust to enter over periods of many years, making them ideal sampling sites. The selected sites in the Free State (FS) province were its capital, Bloemfontein, which is located in the central FS, Kimberley which lies on the FS western border, and Vanderbijlpark in the north, as shown in Table 1 and corresponding maps in Figs. 1 and 2.

A Black & Decker 7.2 V cordless wet and dry Dust Buster handheld vacuum cleaner was used, specifically for its gentle suction action. Some precautions were taken during sampling, e.g. not to collect towards the sides of roofs, not in isolated areas, or where degrading wood and insulation fibers, etc., accumulated. After sampling, the dust samples were sieved through a small sieve (700 µm) to remove larger particles from the smaller dust particles. Table 1 lists precise sampling locations, i.e. suburbs and coordinates—all in residential areas. In Bloemfontein, four sites were identified and sampled, namely in the attics of houses in Langenhovenpark (LHP) directly west of the main north–south national N1 highway, Universitas (U) directly east of the N1, Heidedal (H) that lies next to the city's industrial area, and Maselspoort (M) that lies to the east of the city, but where the municipality's water purification works is located. The two sites west and east of the N1 highway were selected to investigate possible differences resulting from mainly westerly winds that blow in this area.

In Kimberley, three sites were identified and sampled, namely Casandra (C), South Ridge (SR), and Monument Heights (MH). Casandra is located immediately north of the Ekapa mine and the provincial road (R64), west of the De

Table 1 Locations of sampling sites, coordinates displayed in decimal minutes, negative longitude (south), positive latitude (east)

Suburb	City	Coordinates (Longitude, Latitude)
Langenhovenpark (LHP)	Bloemfontein—West	– 29.103, 26.162
Universitas (U)	Bloemfontein—West	– 29.096, 26.170
Heidedal (H)	Bloemfontein—East	– 29.142, 26.261
Maselspoort (M)	Bloemfontein—East	– 29.034, 26.404
South Ridge (SR)	Kimberley—South	– 28.771, 24.762
Monument Heights (MH)	Kimberley—South	– 28.767, 24.760
Casandra (C)	Kimberley—East	– 28.741, 24.794
SE3 1 (VB1)	Vanderbijlpark—South	– 26.741, 27.849
SE3 2 (VB2)	Vanderbijlpark—South	– 26.736, 27.850

Fig. 1 Southern Africa map [21] indicating sampling cities circled in red

Beers diamond mine, and northwest of the industrial area. South Ridge and Monument Heights are located between the N8 and N12 national highways immediately north of the Transnet Railway Station and northwest of the Airport.

Vanderbijlpark was selected for being located in a high-pollution industrial area. Two sites were sampled here, both at the SE3 suburb about 10 km south of the huge ArcelorMittal Steel and other engineering works.

All samples were analyzed by the techniques described here below.

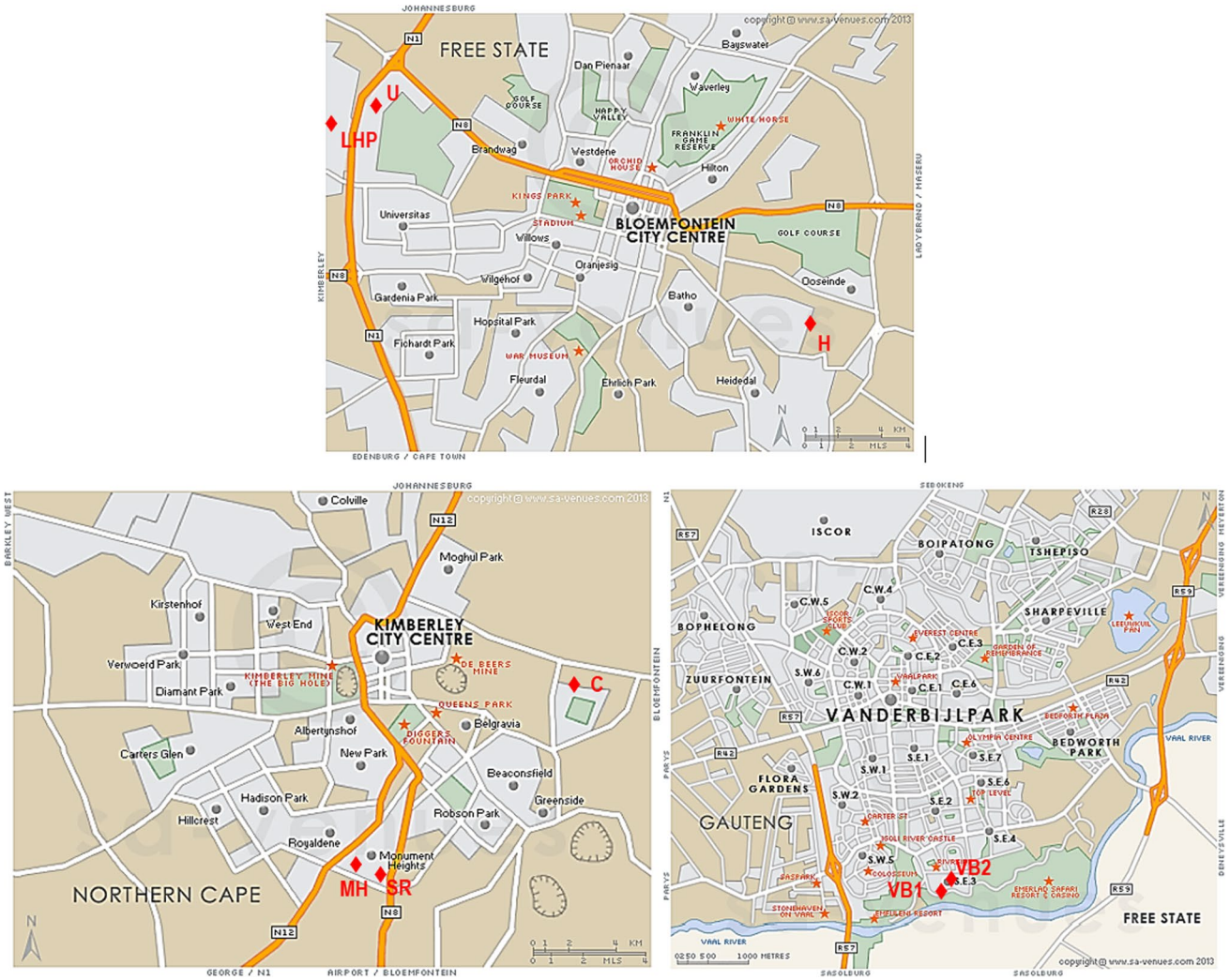

Fig. 2 Sampling sites (♦) and surroundings in Bloemfontein (*top*: 4 sites, with the Maselspoort site not shown—located *ca* 24 km directly northeast of the city center), Kimberley (*bottom left*: 3 sites) and Vanderbijlpark (*bottom right*: 2 sites) [22]

2.2 Scanning electron microscopy—energy dispersive spectroscopy (SEM–EDS)

SEM–EDS was used as a qualitative method in the current study on all of the collected samples. The elemental composition of individual particles and particle morphology was determined using a Jeol IT-200 SEM equipped with an energy-dispersive X-ray spectrometer (Jeol IT 2000) and a secondary electron detector (SED) [23]. Samples were prepared by mounting the sample on carbon tape and iridium (Ir) coating, the coating was required for conductivity purposes. Imaging was performed at an accelerating voltage of 5 kV, working distance (*ca* 11 mm), probe current (30 A), and zoom magnifications varied from 27 to 7500 times. EDS was performed at 15 kV accelerating voltage, working distance *ca* 10 mm, 9 nA probe current, and 60 s acquisition time.

2.3 X-ray fluorescence (XRF)

The major elements (namely Fe, Mn, Ti, Ca, K, S, P, Si, Al, Mg, and Na) were analyzed on a fusion bead containing 2 g of total suspended particles (TSP), and flux lithium borate. A Panalytical Axios XRF spectrometer with a 4-kW rhodium (Rh) tube was used. H_2O loss was determined by measuring mass loss after heating the sample to 110 °C, and loss on ignition (LOI) after

heating the sample to 800 °C. The lower limit of detection for major oxides is 0.01 wt % [24]. This analysis was performed on all collected samples.

2.4 X-ray diffraction (XRD)

Portions of each sample were milled in a carbon steel puck and ring mill, for 10 min, which were then added to a standard sample holder or a zero-background sample holder. Mineral analyses were carried out using a Panalytical Empyrean X-ray Diffractometer. The X-ray source is of copper (Cu) composition and the detector is an X-Celerator detector. The tube geometry configuration has a Bragg–Brentano geometry with a theta-theta goniometer configuration. Analyses were performed from 3.5° to 70° 2θ with tube settings of 45 kV and 40 mA. Data Collector v. 3.0 c and Highscore v. 3.0e software packages were used, equipped with the ICDD PDF-2 database for evaluation of diffractograms [25].

2.5 Electron probe micro analysis (EPMA)

Small portions of each sample were mixed with epoxy (Clarofast) to form an epoxy mount, which was then polished using silicon carbide powders (600 and 120 µm) and diamond suspension (6 and 3 µm). These epoxies were carbon sputter coated using a Quorum Q150, while the minerals were analyzed by using a Jeol JXA-iSP100 EPMA equipped with a tungsten filament with a Jeol energy dispersive X-ray spectrometer (EDS) detector. Analysis conditions were 15 kV acceleration voltage, 10 nA beam current, 60 s analysis time, and 11.1 mm working distance.

2.6 Geographical air mass origins

PM fractions are often transported over long periods and/or long distances. Similarly to what has been done in other local and international studies, the geographical origins of air masses that passed the 3 cities (Bloemfontein, Kimberley, and Vanderbijlpark) were applied as surrogates for long-range transported (LRT) air pollution from distant source areas [6, 7, 26–29]. The Hybrid Single Particle Lagrangian Integrated Trajectory (HYSPLIT) software program was used to generate 72 h backward trajectories every day for the years 1972, 1982, 1992, 2002, 2012, and 2022 for the three cities. The software was downloaded from the National Oceanic and Atmospheric Administration Air Resource Laboratory (NOAA ARL) website [30]. The same method was followed in previous studies [27, 28, 31]. As also used by the National Centers for Environmental Prediction (NCEP) and the National Center for Atmospheric Research (NCAR), Global Reanalysis Meteorological Data from the NOAA ARL were employed. Six-hour intervals (00:00, 06:00, 12:00, and 18:00) were generated from analysis fields (2.5°×2.5° resolution, 17 vertical levels, 10,000 m AGL), while wind fields were linearly interpolated between each interval [27, 28, 32]. Since a single backward trajectory has a large uncertainty and is of limited significance, an ensemble of trajectories with a 500 m starting height and a fixed offset grid factor of 250 m was used in this study (heights of 250 m and 750 m were also used), as done in other studies [7, 26, 28, 32]. In total, 26316 individual backward trajectories were generated for each city for the years 1972, 1982, 1992, 2002, 2012, and 2022. The number of trajectories per year per city was 4380 or 4392, depending on whether the year was a leap year (366 days). These individual backward trajectories were applied in the K-means cluster analysis, which was performed with HYSPLIT software. The K-means cluster method obtains the mean trajectory path of individual backward trajectories. The optimal number of clusters was determined by using a total spatial variance (TSV) plot generated by the HYSPLIT software program (HYSPLIT Tutorial, 2023). For all 3 cities and 6 years, four LRT clusters were identified as the optimal number of clusters.

3 Results and discussion

A total of seventeen elements (C, O, Ti, Fe, Ca, Mg, Al, Si, Cl, K, Ag, S, Cu, Na, Zn, Mn, and Ir) were qualitatively found for the nine SEM–EDS samples in the current study. The presence of Ir was due to metal coating, while C and O most likely resulted from surface contamination and/or the used carbon tape. The most common minerals (geogenic and anthropogenic) that were identified were quartz and feldspars, making it difficult to determine the exact sources of these minerals. The reason is that these minerals are found in most rocks in Southern Africa, with feldspars being the most common group of minerals within the continental crust, and quartz being the second.

LRT clusters combined with mineralogical analyses pointed to the Bushveld Complex, the Karoo-, Olifantshoek-, Cape- and Transvaal Supergroups, and the Hardveld Land Division (Botswana) being prominent sources in Southern Africa (a brief description of the mentioned Supergroups is included in the Supporting Information). As one of the most active mining countries in the world, the large mining industry in South Africa necessitates more related PM pollution research. During morphology and elemental composition studies of suspended dust/particulate matter, microscopy was found to be a useful complement in the analyses of particle size and mineral composition.

3.1 Scanning electron microscopy and energy dispersive spectroscopy (SEM–EDS)

SEM–EDS is an analytical technique that is ideally suitable for investigations of sample and material surfaces. Elemental compositions of individual particles and particle morphologies were determined for the nine samples collected in this study. All dust samples were mounted in their original sample states during SEM–EDS analyses. Analyses therefore include results in their entirety, i.e. composed of both inorganic and possible organic constituents. The presence of Ir in the samples is ascribed to the coating of samples as required for SEM analyses, while carbon results from the tape that was used.

Various particle morphology images and qualitative elemental compositions for the four sites in and outside Bloemfontein, i.e. LHP, U, H & M, were taken at magnifications varying from 35 to 750 times, see Figures S1–S8 in the Supporting Information. The two sites west (LHP) and east (U) of the N1 highway were selected to investigate possible differences because of mainly westerly winds that blow in the central Free State, with more PM possibly resulting from heavy traffic expected downwind, i.e. in U. However, no significant differences were observed between the elemental composition for all three sites, LHP, U, and H located inside the city residential areas. Also, no chlorine species were found directly next to the municipal waterworks at M, which is known for its use of ample amounts of $Ca(OCl)_2$ during the decontamination process. Dissolved hypochlorite ions (OCl^-) in the water mass are in equilibrium with the formed hypochlorous acid (HOCl), which serves as a disinfectant. Over time, both hypochlorous acid and hypochlorite ions decompose to form chloride (Cl^-) ions and oxygen (O_2), particularly when exposed to sunlight or organic matter. After calcium hypochlorite is added and dissolved, water volumes are typically moved into closed systems such as contact tanks or pipes where it is retained for a certain period, ensuring effective disinfection contact time. Hereafter treated water is stored in covered reservoirs or pumped directly into the distribution network through closed pipes and tanks, which helps maintain residual chlorine levels and prevents external contamination. The release of chlorine species into the atmosphere and its presence in neighboring dust deposits are thus not expected, as unambiguously established in this study.

Figures 3 and 4 show SEM images and EDS spectra with qualitative elemental compositions of samples from the LHP and M sites. Only at Maselspoort (M), located at *ca* 24 km northeast of the city center, one difference was observed in the elemental composition, i.e. Zn was also observed here.

Particle morphology images for the SR site in the mining city Kimberley were taken at magnifications ranging from 33 to 190 (see Supporting Information, Figure S9), for the MH site at magnifications ranging from 35 to 230 (SI: Figure S11), and for the C site at magnifications ranging from 37 to 160 (SI: Figure S13). The EDS spectra for the SR, MH, and C sites are shown in Figs. 5, 6, 7, while corresponding elemental compositions are shown in SI: Figures S10, S12, and S14 respectively. The same level of similarity was not observed for the Kimberley sites as in Bloemfontein, e.g. no sodium (Na) was detected in samples from the Kimberley sites, as opposed to both the Bloemfontein and Vanderbijlpark sites. The key difference at the Kimberley sites was the SR site did not contain Cl but did contain Cu, which in turn was not observed at the other Kimberley sites. The MH site indicated Cl, and uniquely also Ag, while Cl was also observed at the C site.

EDS spectra (elemental compositions) of samples from the SE3 1 & 2 sites in Vanderbijlpark are shown in Figs. 8 and 9, while corresponding elemental compositions are illustrated in Figures S16 and 17 in the Supporting Information. Particle morphology images for the SE3 1 and SE3 2 sites were taken at magnifications ranging from 30 to 85 (SI: Figure S15) and magnifications ranging from 55 to 150 (SI: Figure S17), respectively. Of all nine samples, the SE3 1 site is the only one that indicated Mn. Modeling results of the origins of the various dust samples presented here are shown in Sect. 3.6 below.

In summary, the major elements found in each sample were sodium, magnesium, aluminum, silicon, sulfur, potassium, calcium, titanium, and iron. Contrary to the other sites, the Kimberley site indicated no Na, while Cl was found at LHP, H, MH, C, SE3 1, and SE3 2. Mn was found only at SE3 1, and Cu at SR, MH, SE3 1 and SE3 2. Zn was only found

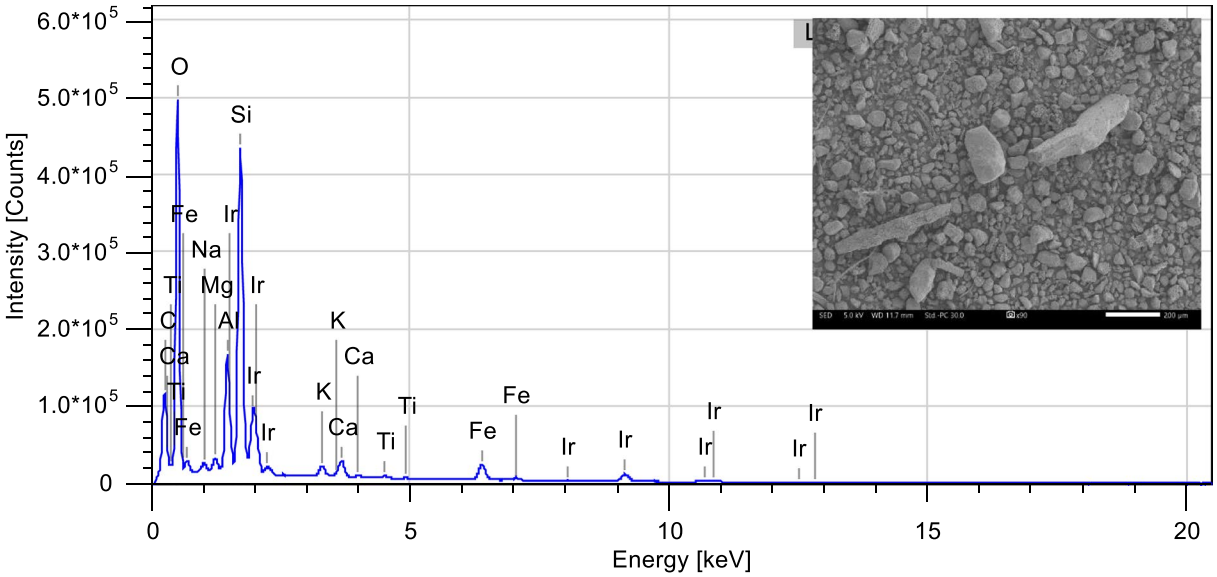

Fig. 3 Secondary electron image (SEI) and EDS spectrum showing the qualitative elemental composition of the sample taken at the LHP site, Bloemfontein. ×90, 200 µm scale (indicated by the white bar), 30.0 probe current (PC), 11.7 mm working distance (WD), 5.0 kV accelerating voltage

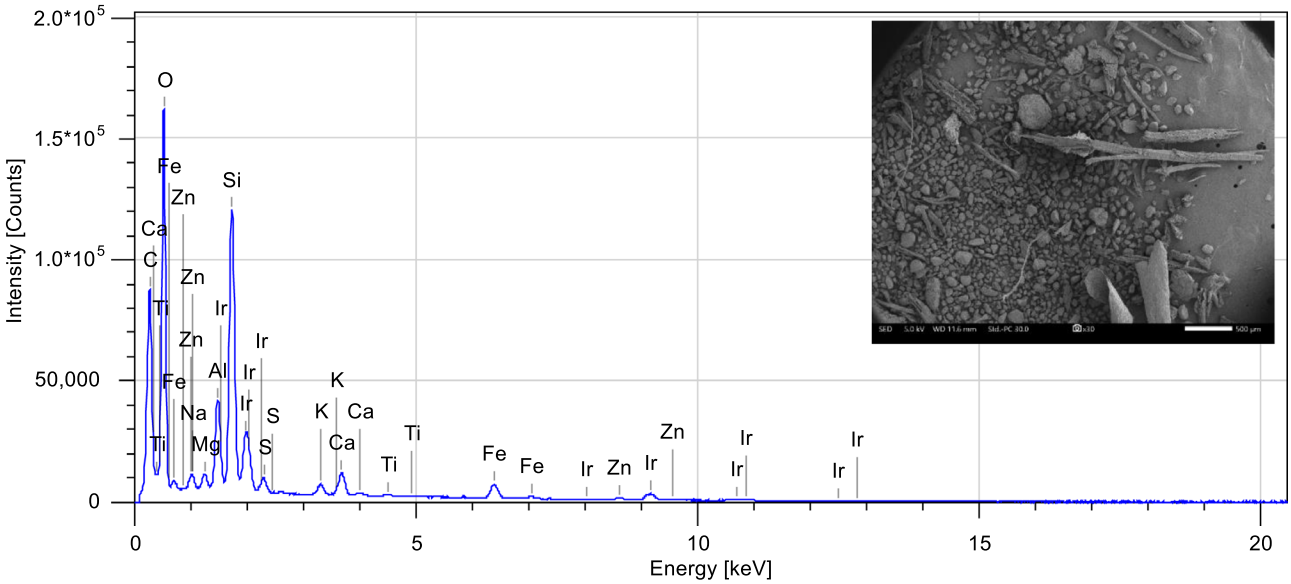

Fig. 4 Secondary electron image (SEI) and EDS elemental composition observed at the M site, Bloemfontein. ×30, 500 µm scale (indicated by the white bar), 30.0 probe current (PC), 11.6 mm working distance (WD), 5.0 kV accelerating voltage

at M, and Ag only at MH. The presence of carbon and oxygen is ascribed to the thin contamination layer of organic molecules that form on the sample surface during handling and imaging.

3.2 X-ray fluorescence (XRF)

XRF studies found the main constituents of all the dust samples to be SiO_2, Al_2O_3, Fe_2O_3, and CaO, see Fig. 10. The Maselspoort sample was the only one that would not fuse, consequently, XRF analysis could not be done for this sample.

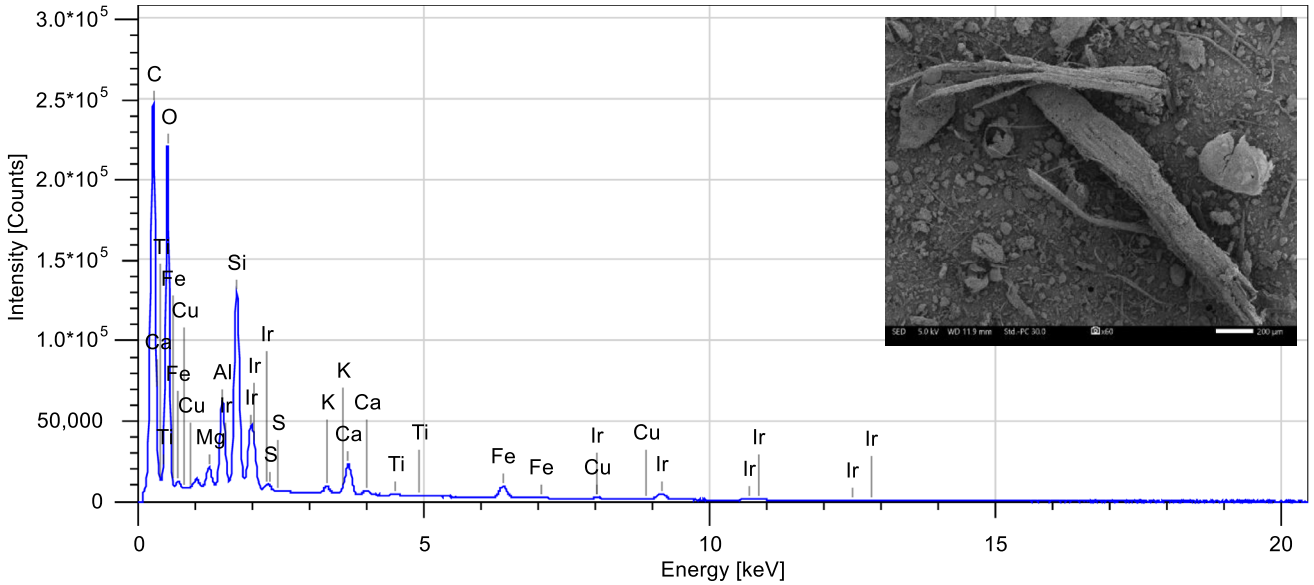

Fig. 5 Secondary electron image (SEI) and EDS elemental composition observed at the SR site, Kimberley. ×60, 200 µm scale (indicated by the white bar), 30.0 probe current (PC), 11.9 mm working distance (WD), 5.0 kV accelerating voltage

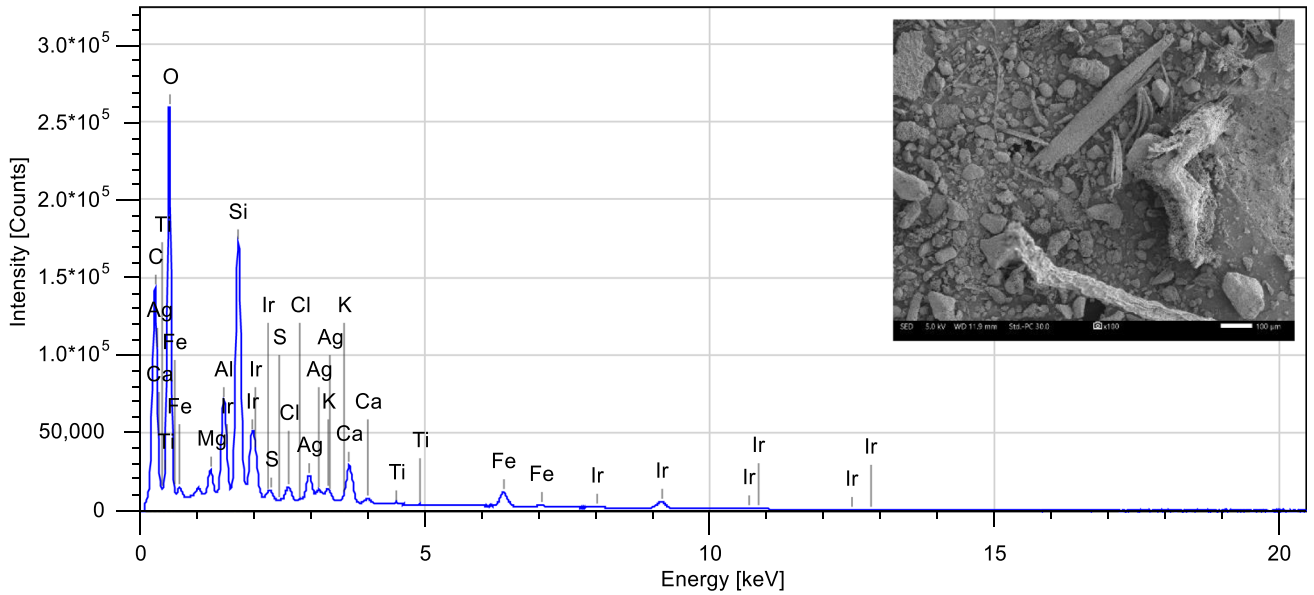

Fig. 6 Secondary electron image (SEI) and EDS elemental composition observed at the MH site, Kimberley. ×100, 100 µm scale (indicated by the white bar), 30.0 probe current (PC), 11.9 mm working distance (WD), 5.0 kV accelerating voltage

3.3 X-ray diffraction (XRD)

XRD results (Fig. 11, Table S2, and Figures S19–S27) show the samples to be mostly composed of silicates; quartz (silicon dioxide), plagioclase (variations from $NaAlSi_3O_8$ to $CaAl_2Si_2O_8$) and/or K-feldspar (aluminosilicates). Figure 11 illustrates the mineral distribution, with quartz, plagioclase, and K-feldspar representing 55–89% of the samples. The Bloemfontein samples (LHP, U, H, and M) are more complex when compared to the Vanderbijlpark (SE3 1 and SE3 2) and Kimberley (SR, MH, and C) samples. After the silicate mineral component, the next most prominent component is the carbonates. The main mineralogical constituents of all samples are quartz and plagioclase, followed by minor

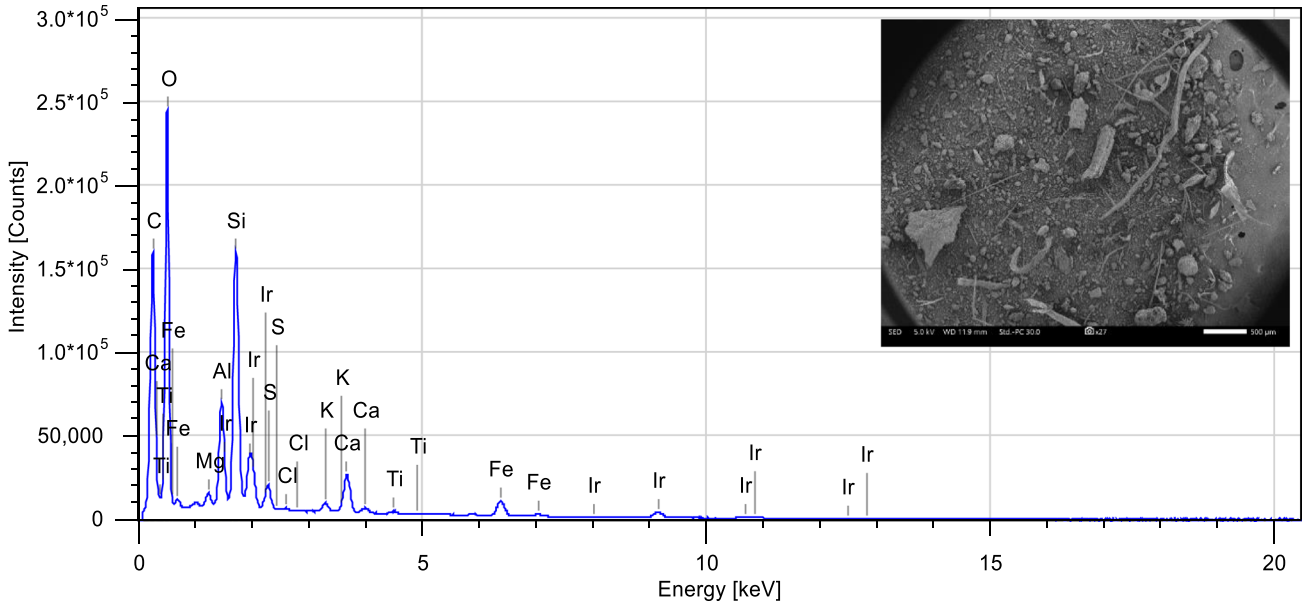

Fig. 7 Secondary electron image (SEI) and EDS elemental composition observed at the C site, Kimberley. ×27, 500 µm scale (indicated by the white bar), 30.0 probe current (PC), 11.9 mm working distance (WD), 5.0 kV accelerating voltage

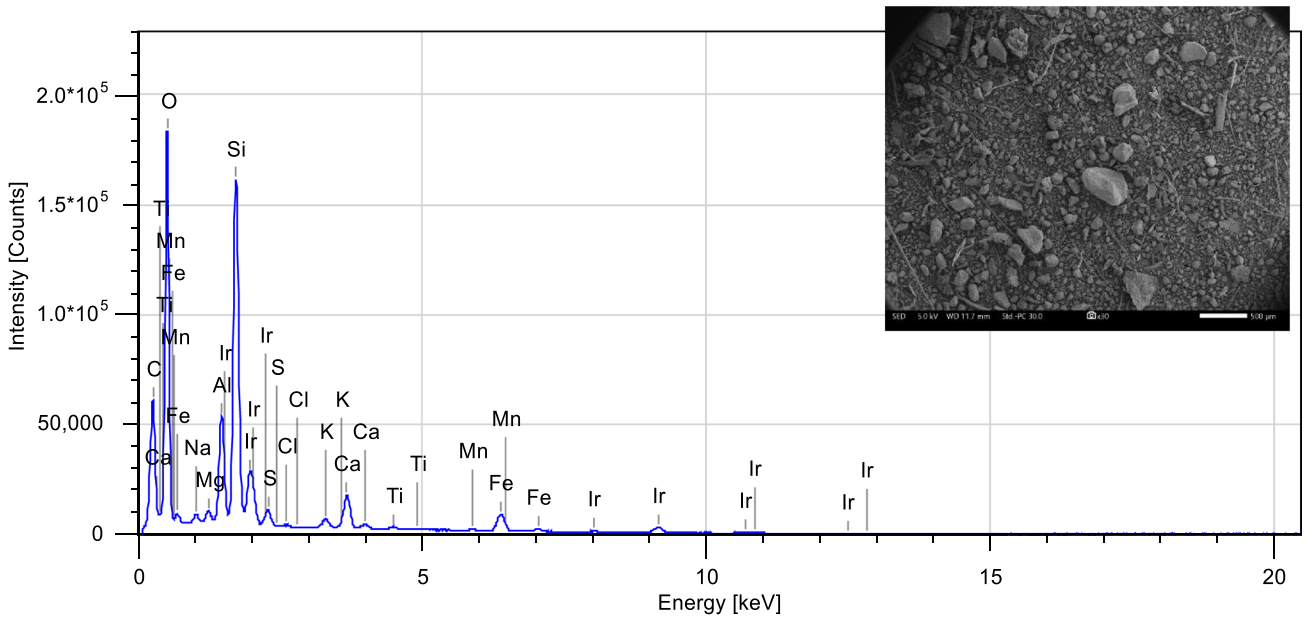

Fig. 8 Secondary electron image (SEI) and EDS elemental composition observed at the SE3 1 site, Vanderbijlpark. ×30, 500 µm scale (indicated by the white bar), 30.0 probe current (PC), 11.7 mm working distance (WD), 5.0 kV accelerating voltage

amounts of calcite, ankerite, stilbite, ilmenite, anatase, goethite, k-feldspar, magnetite, mica, hematite, kaolinite, and gypsum.

3.4 Electron probe micro analysis (EPMA)

The intention of completing the analyses for the current study through the EPMA technique was to determine the minerals that may be present at concentrations too low to be detected by XRD. Large amounts of quartz and silicate

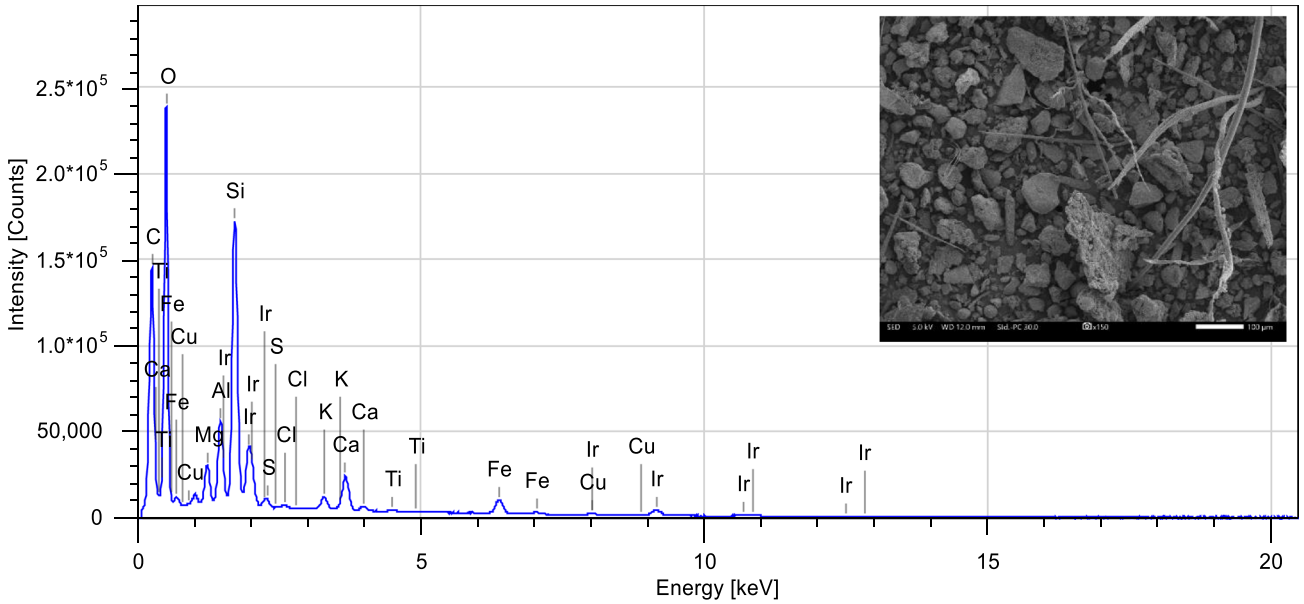

Fig. 9 Secondary electron image (SEI) and EDS elemental composition observed at the SE3 2 site, Vanderbijlpark. ×150, 100 µm scale (indicated by the white bar), 30.0 probe current (PC), 12.0 mm working distance (WD), 5.0 kV accelerating voltage

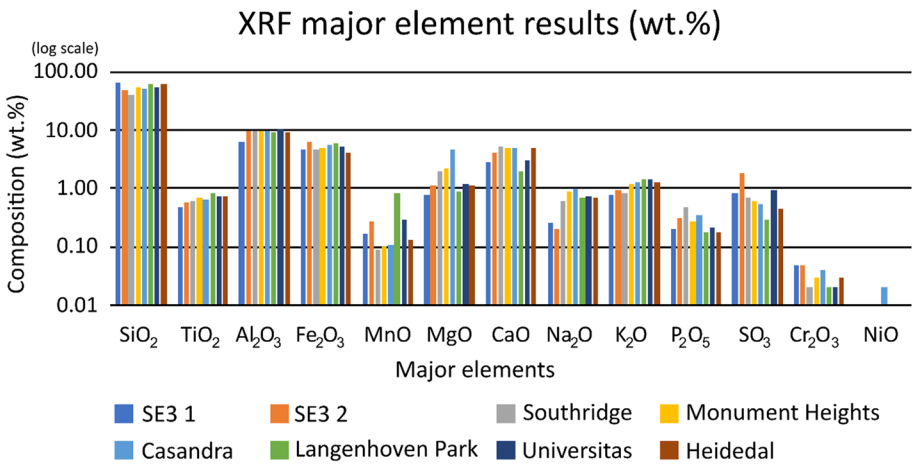

Fig. 10 X-ray Fluorescence results, corresponding to Table S3 in the Supporting Information (logarithmic scale y-axis)

minerals (such as plagioclase and pyroxene) are present in all samples, which was expected. Pyroxene was only detected using EPMA analysis, due to concentrations too low for XRD analysis.

The samples from Vanderbijlpark have Fe-minerals present in addition to the silicates. These Fe-minerals are pyrite, magnetite/hematite, and Fe-metal. The samples from the Kimberley area contain small quantities of chromite, magnetite/hematite, ilmenite, and Fe-metal, see Fig. 12. The samples from the Bloemfontein area contain minerals similar to those found in the Kimberley area, with Maselspoort containing also Zn-minerals and barite. Analytical data of these minerals may be viewed in the Supporting Information (Table S3).

3.5 Interpretation of XRD, EPMA and HYSPLIT

South Africa is a mineral-rich country with an extensive mining industry spread across the country. Combining LRT clusters with the minerals identified in the samples of the present study, as well as mining and anthropogenic sources, provides a means to help locate the origins of the dust samples [33].

Table 2 shows the different minerals found in the samples, the most probable sources, and the source areas from the HYSPLIT maps. The minerals that were identified are generally common. The identified sources correspond to the source of the HYSPLIT cluster results. The quartz and feldspars found in the samples are abundant earth crust

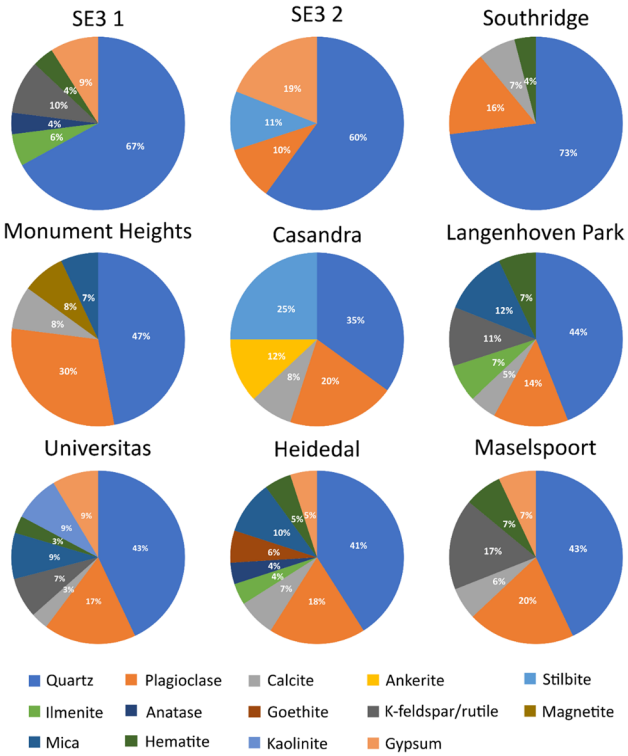

Fig. 11 X-ray Diffractometer (XRD) results, corresponding to Table S1 in the Supporting Information

minerals, thus making it difficult to attribute their specific origins [34]. Large areas of the South African landscape are covered by the Karoo Supergroup, which consists of layers of sedimentary rocks capped by basalts [35]. Minerals such as quartz, plagioclase, clay minerals, pyroxene, K-feldspar, gypsum and mica are present in the Karoo Supergroup [35]. Amygdales in the basalts may be the source of stilbite [35]. The Cape- and Olifantshoek Supergroups also consist of sedimentary rocks, which are partially metamorphosed [35, 36].

The groups in the Transvaal Supergroup that became of interest in this study are the Banded Iron Formation (BIF) rocks and the limestones, which may be the sources of the Fe minerals, hematite and magnetite, and the carbonates respectively [37].

The Bushveld Complex (BC) is South Africa's source of platinum, which is found in ultramafic rocks and chromitite layers [38]. These rocks consist mainly of pyroxenes, plagioclases, K-feldspars, and chromites (Chaumba 2022). The BC, as well as discarded mine wastes, may be sources of chromites, ilmenite, rutile, magnetite, and olivine.

Due to the proximity of the Kimberley samples, it is important to note that ilmenite, pyroxene, and calcite are also found in kimberlites [39]. The Hardveld Land Division (Botswana) consists of sedimentary rocks (metamorphosed siliciclastic), basalt, and granite gneisses [40]. This area is a source of dust in the Kimberley area, which is mostly a farming vicinity.

3.6 LRT clusters

For the present studies, the Free State Province (FS) was selected due to the virtual absence of previous investigations related to PM pollution within the province. As an area with a higher level of population in the FS, being centrally located, lying within an extended agricultural land area, and situated at the intersection of main highway and railway lines, the capital, Bloemfontein, was first selected. Extensive grain cultivation dominates the landscape to the north and west of Bloemfontein, with large fields frequently plowed. For purposes of comparison, the diamond mining city of Kimberley which lies on the FS-eastern border and directly southeast of some of the world's largest iron and manganese-producing mines was also selected. Lastly, the traditionally heavy steel industry town of Vanderbijlpark in the north was also added. This town lies between the high-pollution industrialized Gauteng province Witwatersrand area to its north and Sasolburg with its many fossil fuel-based chemical industries. With all these variables in mind, the aim was to also determine changes in air mass transport clusters over the past five decades (1972, 1982, 1992, 2002, 2012, and 2022), at 10-year intervals. These changes are shown in Table 3 and Figs. 13, 14, 15.

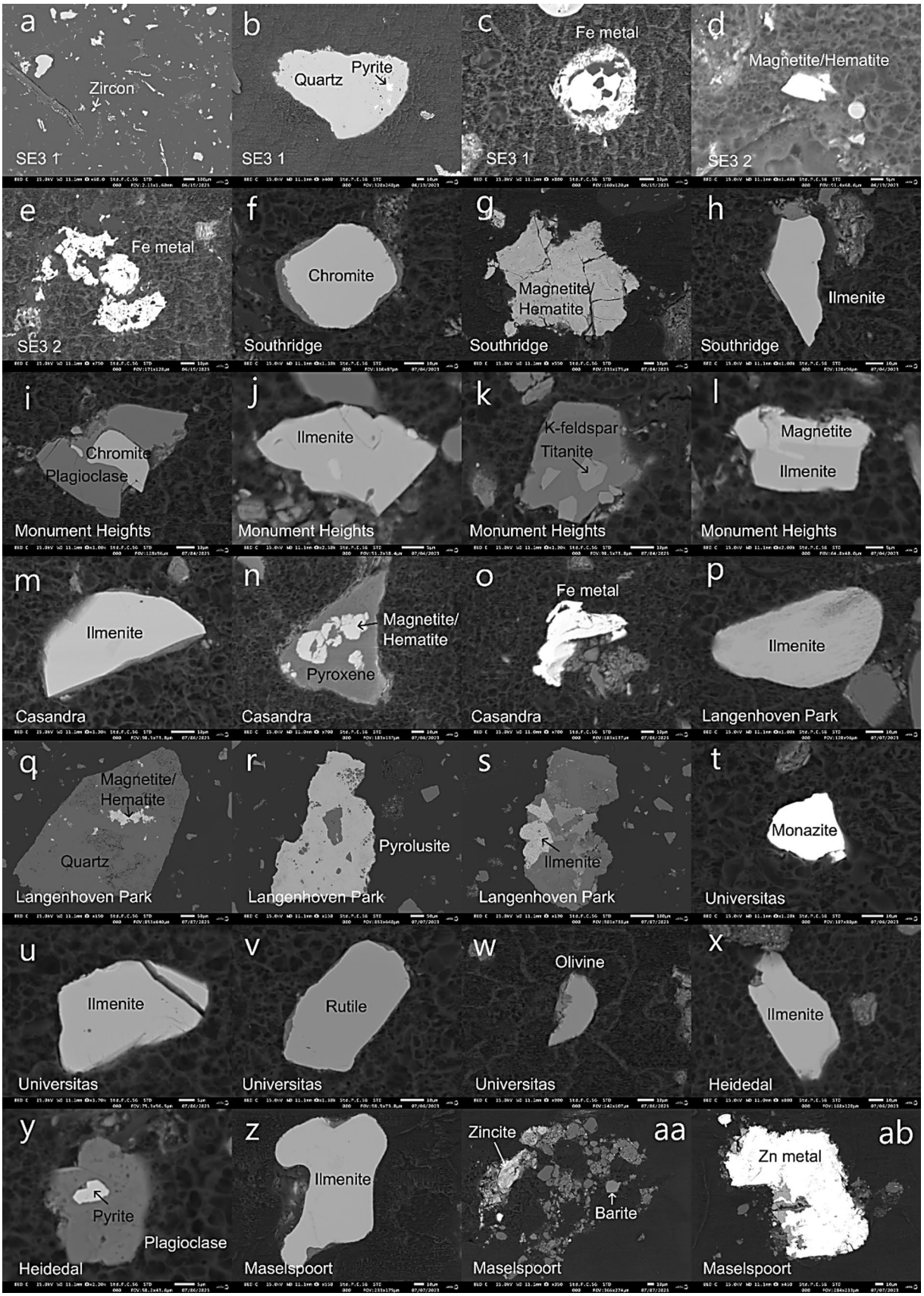

Fig. 12 Electron Probe Microanalysis images of the minor minerals within the dust samples. Analytical results are listed in Table S3

Table 2 Minerals detected in samples, and possible sources according to the HYSPLIT data

Area	Sample	Minor/trace minerals	Possible sources	HYSPLIT data suggested source
Bloemfontein	Langenhovenpark	Hematite	Sedimentary/Fe ore	Karoo supergroup, Bushveld complex, Olifantshoek supergroup, Cape supergroup
		Magnetite/Hematite	Bushveld complex/Fe ore	
		Pyrolusite	Mn fields	
	Universitas	Hematite	Sedimentary/Fe ore	
		Gypsum	Sedimentary	
		Rutile	Heavy mineral sands	
		Olivine	Bushveld complex/Kimberlite	
	Heidedal	Anatase	Heavy mineral sands/granites	
		Hematite	Sedimentary/Fe ore	
		Pyrite	Witwatersrand gold fields	
	Maselspoort	Hematite	Sedimentary/Fe ore	
		Gypsum	Sedimentary	
		Zincite	Bushveld complex	
		Barite	Sedimentary/Bushveld complex	
Kimberley	Southridge	Hematite	Sedimentary/Fe ore	Karoo supergroup, Bushveld complex, Transvaal supergroup, Cape supergroup, Hardveld land division (Botswana)
		Chromite	Bushveld complex	
	Monument Heights	Magnetite	Bushveld complex/Fe ore	
		Chromite	Bushveld complex	
		Titanite	Permatite/skarn deposit	
	Casandra	Magnetite/Hematite	Sedimentary/Fe ore	
		Pyroxene	Bushveld complex/dolerites	
Vanderbijlpark	VB1	Hematite	Sedimentary/Fe ore	Karoo supergroup, Bushveld complex, Olifantshoek supergroup, Transvaal supergroup, Cape supergroup
		Pyrite	Witwatersrand gold fields	
	VB2	Stilbite	Basalts	
		Magnetite/Hematite	Sedimentary/Fe ore	

Table 3 Long-range transport (LRT) clusters for each location in the years 1972, 1982, 1992, 2002, 2012, and 2022

	Cluster	1972	1982	1992	2002	2012	2022
Bloemfontein	1	MP (30%)	NW (41%)	Lesotho (29%)	NW (29%)	FS (40%)	NC (25%)
	2	NW (25%)	NC (29%)	NW (37%)	WC (20%)	NC (27%)	WC (31%)
	3	NC (25%)	FS (19%)	NC (22%)	FS (36%)	L (20%)	L (16%)
	4	EC (20%)	WC (11%)	AO (12%)	L (15%)	EC (12%)	FS (28%)
Kimberley	1	NC (31%)	Limpopo (32%)	NW (43%)	AO (21%)	NC (31%)	NC (25%)
	2	L (31%)	NC South (31%)	EC (17%)	FS (32%)	FS (27%)	FS (28%)
	3	WC (23%)	FS (21%)	NC (21%)	L (17%)	Botswana (25%)	Botswana (34%)
	4	Lesotho (15%)	NC North (16%)	AO (18%)	Botswana (31%)	WC (18%)	L (13%)
Vanderbijlpark	1	MP (41%)	L (35%)	MP (38%)	NW (37%)	MP (40%)	L (48%)
	2	NW (27%)	MP (23%)	WC (13%)	NC (12%)	L (21%)	FS (23%)
	3	IO (19%)	KZN (21%)	NW (18%)	MP (38%)	FS (34%)	KZN (22%)
	4	NC (13%)	NW (21%)	L (31%)	KZN (14%)	WC (5%)	NC (7%)

Cluster-relevant geographical areas are the neighboring countries of Lesotho and Botswana, the Atlantic (AO) and Indian (IO) Oceans, and the North-West (NW), Eastern Cape (EC), Northern Cape (NC), Free State (FS), Limpopo (L), Western Cape (WC), KwaZulu-Natal (KZN), and Mpumalanga (MP) provinces of South Africa.

Using backward trajectories, changes in the origins of air masses over five decades could be determined for the three main locations, Bloemfontein, Kimberley, and Vanderbijlpark. The four most prominent clusters of air mass origins are shown for each specific year, in Table 3. The cluster origins in 1972 for Bloemfontein were Mpumalanga (MP), North West (NW), Northern Cape (NC), and the Eastern Cape (EC). Except for the NC, five decades later these clusters changed almost completely, namely to NC, Free State (FS), Limpopo (L), and the Western Cape (WC). The cluster origins in 1972 for Kimberley were the Northern Cape (NC), Limpopo (L), Western Cape (WC), and Lesotho. Over five decades two of these clusters changed, i.e. the WC and Lesotho were replaced by the FS and Botswana. The cluster origins in 1972 for Vanderbijlpark (Gauteng province) were Mpumalanga (MP), NW, the Indian Ocean (IO), and NC. Fifty years later these cluster origins changed to L, FS, Kwa-Zulu Natal (KZN), and NC. It is thus seen that between 1972 and 2022 the directions of air currents changed significantly, resulting in changes in the contribution of different sources to attic dust composition. The origins of the air masses show that the dominant movement in 2022 in Bloemfontein (averaging 51% over the five-decade period) and Kimberley (averaging 52% over the five-decade period) is in the north-easterly and south-westerly directions, whereas prominent directions experienced in the Vanderbijlpark (averaging 52.5% over the five-decade period) region were east–west.

4 Conclusions

General particle composition and mineral elemental analysis pointed to dust PM essentially consisting of similar components, regardless of its various origins. The most common PM mineral found was quartz, as expected from it being the most common mineral in the earth's crust. Regardless of having chosen sampling sites close to heavy industries, chlorine treatment water works, mines, and heavy road traffic, typical pollutants from these potential sources were absent or hardly detected. This may be ascribed to the high volatility of some pollutants or tiny sizes typically associated with these sources, which otherwise did not settle in measurable quantities on ceilings of houses in residential areas.

From air mass geographic origin investigations, i.e. LRT cluster analyses, clusters changed significantly over the five decades for each of the three cities of this study. These clusters were used as indicators of PM distant source areas. Detection of changes in the geographic origins of air masses is important in studies of this kind.

While this study provides significant insights into the chemical composition and the possible geographical origins of residential attic dust in Central South Africa, it is important to acknowledge the limitations of the analytical techniques employed. The use of EPMA, XRD, XRF, and SEM allowed us to analyze the elemental composition and mineral phases of the dust particles, but each technique has its inherent constraints. For instance, the detection limits of XRD restrict the detection of trace mineralogy, thus potentially underestimating the presence of minor pollutants. Furthermore, these techniques focus on elemental and phase analysis and do not offer detailed insights into the chemical speciation

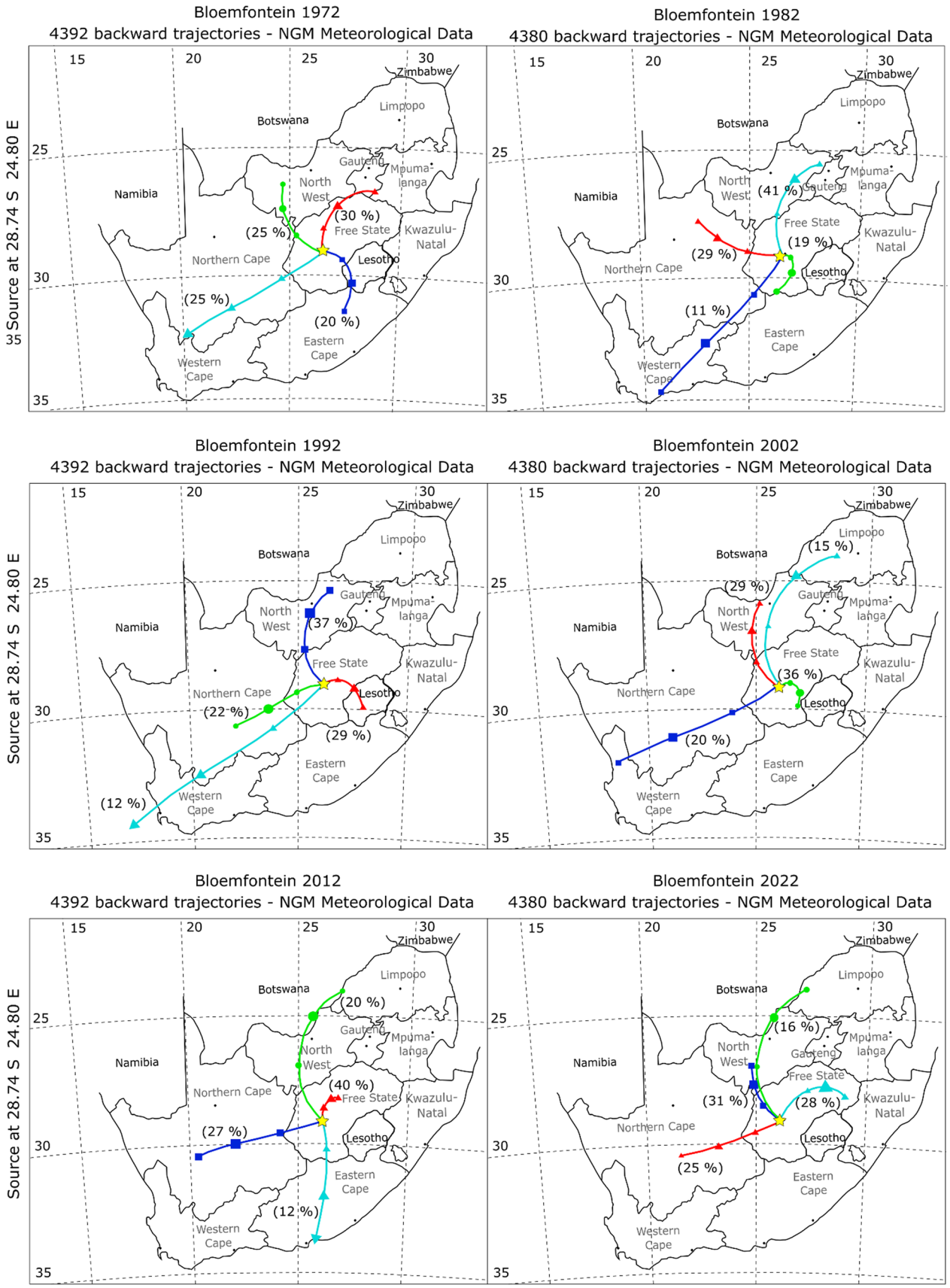

Fig. 13 LRT clusters determined for Bloemfontein (Free State province) over 5 decades

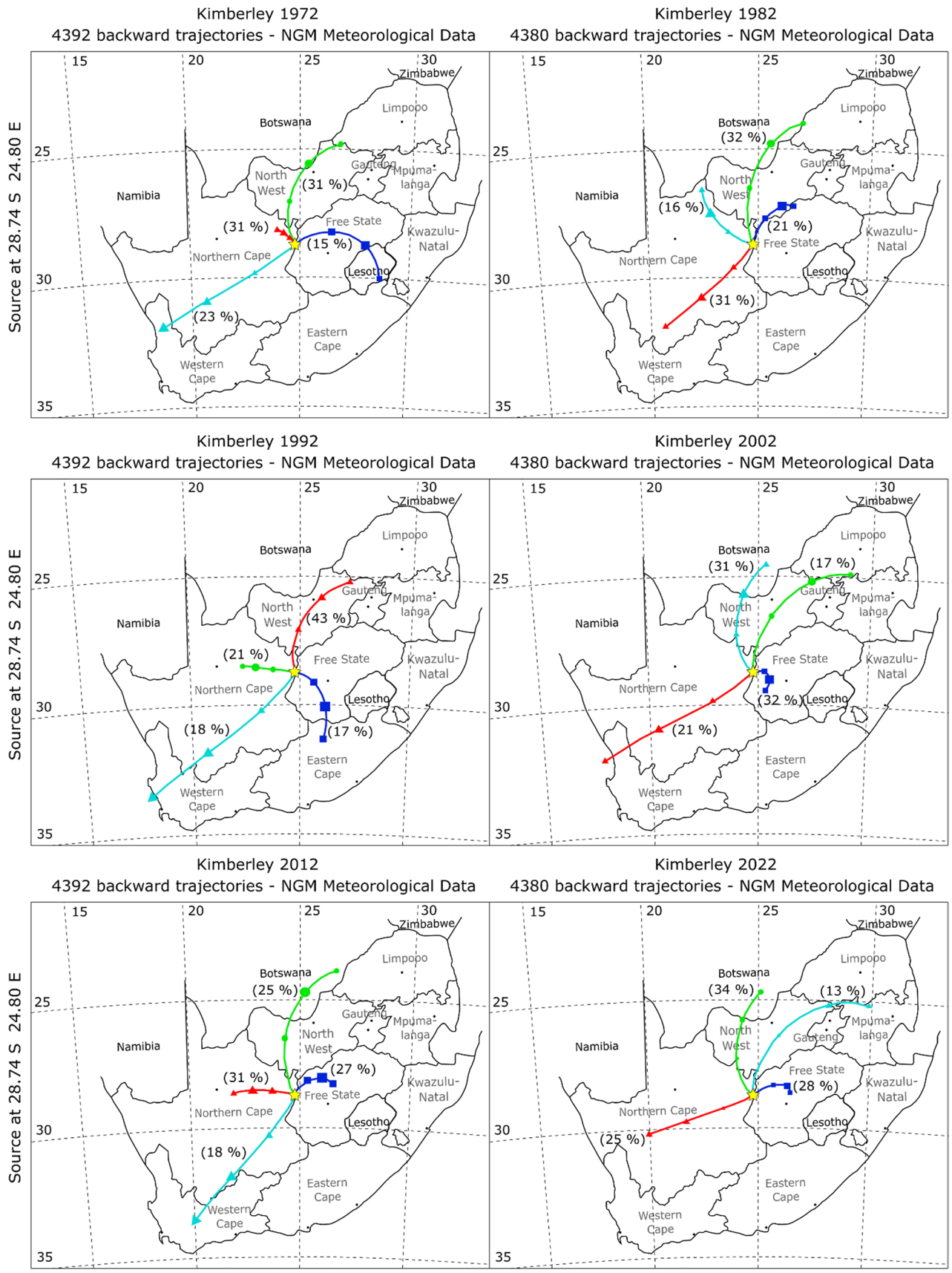

Fig. 14 LRT clusters determined for Kimberley (Northern Cape province) over 5 decades

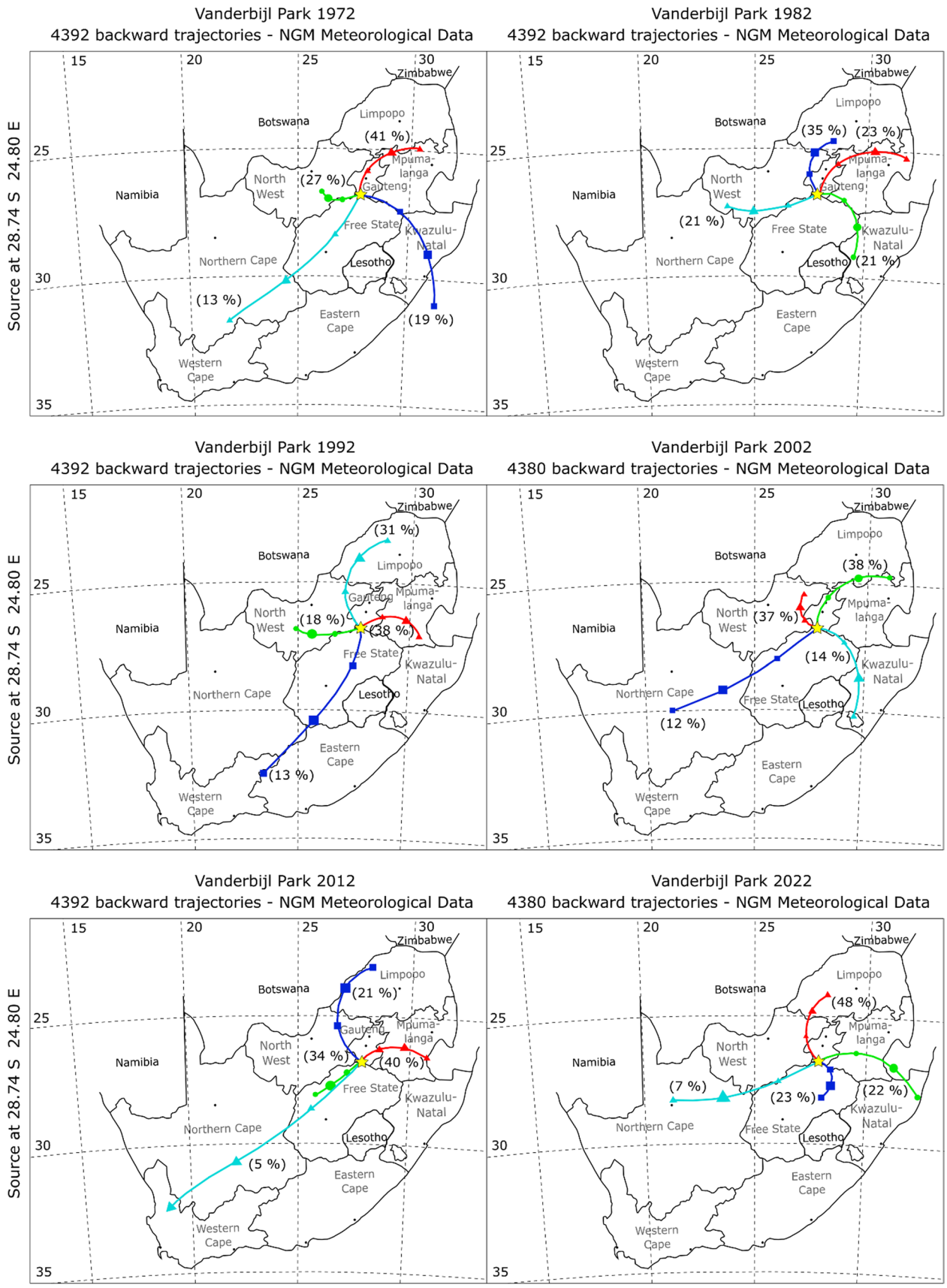

Fig. 15 LRT clusters determined for Vanderbijlpark (Gauteng province) over 5 decades

or bioavailability of the elements that were detected. These properties may have significant environmental or health implications, and should thus be considered in future studies.

Additionally, while HYSPLIT provided valuable data on the potential transport pathways of dust particles since 1972 (every 10 years), its model is based on meteorological data, which may not fully capture the complexities of dust movement, particularly for larger dust particles in heterogeneous terrains or under varying atmospheric conditions. We used three starting heights (250 m, 500 m & 750 m), similar to other studies [6, 7, 26, 28, 29]. The HYSPLIT software has inherent limitations, e.g. it does not incorporate the effects of complex terrain or particle transport [30]. Additionally, the meteorological data used in the HYSPLIT software are available at relatively coarse temporal resolution (1–6 h), which can result in errors in rapidly changing conditions.

This study assists in improving the understanding of the composition of attic dust in terms of the minerals and other PM pollutants it may carry. Additional studies in South Africa may be done in the future, such as determining the presence and phases of pollutants, focusing on specific mineral pollutants, and determining the impact they may have on the environment.

Author contributions Conceptualization and methodology by K.G.v.E.; validation by D.v.d.W. and K.G.v.E.; formal analysis by D.v.d.W., M.W–P.; investigation by D.v.d.W. and M.W–P.; resources by K.G.v.E.; data curation by D.v.d.W. and K.G.v.E.; writing—original draft preparation by D.v.d.W. and K.G.v.E.; writing—review and editing by D.v.d.W., J.W., K.G.v.E. and M.W–P.; visualization by D.v.d.W., M.W–P. and K.G.v.E.; supervision by K.G.v.E. and J.W.; project administration by K.G.v.E. All authors have read and agreed to the published version of the manuscript.

Funding This research was funded by the Central Research Fund of the University of the Free State, Bloemfontein.

Data availability The datasets generated during and/or analysed during the current study are available from the corresponding author on reasonable request.

Declarations

Competing interests The authors declare no competing interests.

References

1. Wang H, Dwyer-Lindgren L, Lofgren KT, Rajaratnam JK, Marcus JR, Levin-Rector A, Levitz CE, Lopez AD, Murray CJL. Age-specific and sex-specific mortality in 187 countries 1970–2010: a systematic analysis for the global burden of disease study. Lancet. 2012;380:2071–94.
2. WHO global air quality guidelines: particulate matter (PM2.5 and PM10), ozone, nitrogen dioxide, sulfur dioxide and carbon monoxide. 2021. https://www.who.int/publications/i/item/9789240034228. Accessed Nov 2024.
3. IPCC. Climate change 2023: synthesis report core writing team. In: Lee H, Romero J, editors. Contribution of Working Groups I, II and III to the sixth assessment report of the intergovernmental panel on climate change. Geneva: IPCC; 2023. p. 35–115.
4. Sarpong SA, Donkoh RF, Konnuba JK, Ohene-Agyei C, Lee Y. Analysis of PM2.5, PM10, and total suspended particle exposure in the tema metropolitan area of Ghana. Atmosphere. 2021;12:700. https://doi.org/10.3390/atmos12060700.
5. Worobiec A, Potgieter-Vermaak SS, Berghmans P, Winkler H, Burger R, Van Grieken R. Air particulate emissions in developing countries: a case study in South Africa. Anal Lett. 2011;44:1907–24. https://doi.org/10.1080/00032719.2010.539734.
6. Adeyemi A, Molnar P, Boman J, Wichmann J. Source apportionment of fine atmospheric particles using positive matrix factorization in Pretoria, South Africa. Environ Monit Assess. 2021;193:716. https://doi.org/10.1007/s10661-021-09483-3.
7. van der Westhuizen D, Howlett-Downing C, Molnár P, Boman J, Wichmann J, von Eschwege KG. Source apportionment of fine atmospheric particles in Bloemfontein, South Africa, using positive matrix factorization. Environ Monitor Assess. 2024;196:88. https://doi.org/10.21203/rs.3.rs-3265323/v1.
8. Howlett-Downing C, Boman J, Molnár P, Shirinde J, Wichmann J. Source apportionment of PM2.5 and PM2.5-bound trace elements in Pretoria, South Africa. Environm Forensics. 2024;25(1):1–15. https://doi.org/10.1080/15275922.2023.2297423.
9. Mathuthu M, Dudu V, Manjoro M. Source apportionment of air particulates in South Africa: a review. Atmosp Climate Sci. 2019;9:100–13. https://doi.org/10.4236/acs.2019.91007.
10. Mioč P, Žnidarčič M. Basic Geological Map of SFR Yugoslavia 1:100.000, Explanatory Text for Maribor and Leibnitz Sheet. Zvezni Geološki Zavod. Beograd. 1989:60.

11. Šoster A, Zavašnik J, Ravnjak M, Herlec U. REE-bearing minerals in Drava river sediments, Slovenia, and their potential origin. Geologija. 2017;60:257–66. https://doi.org/10.5474/geologija.2017.018.
12. Mencin GE, Jamšek RP, Trajanova M, Gale L, Bavec M, Anselmetti FS, Šmuc A. Provenance and morphostratigraphy of the Pliocene-Quaternary sediments, in the Celje and Drava-Ptuj Basins (eastern Slovenia). Geologija. 2017;62:189–218.
13. Hinterlechner RA. Pohorske metamorfne kamenine. Geologija. 1971;14:187–226.
14. Mioč P. Basic Geological Map of SFR Yugoslavia 1:100.000, Explanatory Text for Slovenj Gradec Sheet. Zvezni Geološki Zavod. Beograd. 1978:74.
15. Zupančič N. Petrografske značilnosti in klasifikacija pohorskih magmatskih kamnin. Rudarsko Metalurški Zbornik. 1994;41:101–12.
16. Gaberšek M, Gosar M. Towards a holistic approach to the geochemistry of solid inorganic particles in the urban environment. Sci Total Environ. 2021;763: 144214.
17. Gosar M, Šajn R. Mercury in soil and attic dust as a reflection of Idrija mining and mineralization (Slovenia). Geologija. 2001;44(1):137–59.
18. Miler M, Gosar M. Assessment of contribution of metal pollution sources to attic and household dust in Pb-polluted area. Indoor Air. 2019;29(3):487–98. https://doi.org/10.1111/ina.12548.
19. Šajn R. Factor analysis of soil and attic-dust to separate mining and metallurgy influence, Meža Valley. Slovenia Math Geol. 2006;38(6):735–47. https://doi.org/10.1007/s11004-006-9039-7.
20. Völgyesi P, Jordan G, Zacháry D, Szabó C, Bartha A, Matschullat J. Attic dust reflects long-term airborne contamination of an industrial area: a case study from Ajka, Hungary. Appl Geochem. 2014;46:19–29. https://doi.org/10.1016/j.apgeochem.2014.03.010.
21. South Africa Map. https://southafricamap360.com/south-africa-map. Accessed Nov 2023.
22. Maps. https://www.sa-venues.com/maps/default.htm. Accessed Nov 2023.
23. Lee E, Terblans JJ, Swart HC. The effect of pH on the luminescence properties of Y_2O_3: Bi phosphor powders synthesized using co-precipitation. Vacuum. 2018;157:237–42.
24. Willis F, Feather C, Turner K. Guidelines for XFD analysis, James Willis Consultants CC, Cape Town. 2014:544.
25. Dinnebier RE, Friese K. Modern XRD methods in mineralogy. In: Introduction to the mineralogical sciences. Oxford: Encyclopedia of Life Support Systems; 2013. p. 1–57.
26. Molnar P, Tang L, Sjoberg K, Wichmann J. Long-range transport clusters and positive matrix factorization source apportionment for investigating transboundary PM2.5 in Gothenburg, Sweden. Environ Sci Process Impacts. 2017;19:1270–7. https://doi.org/10.1039/C7EM00122C.
27. Tshehla C, Djolov G. Source profiling, source apportionment and cluster transport analysis to identify the sources of PM and the origin of air masses to an industrialised rural area in Limpopo. Clean Air J. 2018;28:54–66. https://doi.org/10.17159/2410-972x/2018/v28n2a18.
28. Williams J, Petrik L, Wichmann J. PM2.5 chemical composition and geographical origin of air masses in Cape Town, South Africa. Air Qual Atmos Health. 2020. https://doi.org/10.1007/s11869-020-00947-y.
29. Howlett-Downing C, Boman J, Molnár P, Shirinde J, Wichmann J. PM2.5 chemical composition and geographical origin of air masses in Pretoria, South Africa. Water Air Soil Pollut. 2022;233:271. https://doi.org/10.1007/s11270-022-05746-y.
30. NOAA Air Resources Laboratory. https://www.arl.noaa.gov/. Accessed Oct 2024.
31. Draxler RR, Rolph GD. HYSPLIT (Hybrid Single-Particle Lagrangian Integrated Trajectory) Model. 2003. https://www.ready.noaa.gov/HYSPLIT.php.
32. Wichmann J, Sjoberg K, Tang L, Haeger-Eugensson M, Rosengren A, Andersson EM, et al. The effect of secondary inorganic aerosols, soot and the geographical origin of air mass on acute myocardial infarction hospitalisations in Gothenburg, Sweden during 1985–2010: a case crossover study. Environ Health. 2014;13:1–16.
33. Pawloski GA. Quantitative determination of mineral content of geological samples by X-ray diffraction. Am Miner. 1985;70(7–8):663–7.
34. Amulele GM, Lanati AW, Clark SM. The electrical conductivity of albite feldspar: implications for oceanic lower crustal sequences and subduction zones. Am Miner. 2022;107(4):614–24. https://doi.org/10.2138/am-2021-7836.
35. Thamm AG, Johnson MR. The cape supergroup complex. In: Johnson MR, Anhaeusser CR, Thomas RJ, editors. The geology of South Africa. Johannesburg: Geological Society of South Africa; 2006. p. 443–60.
36. Moen HFG. The Olifants Supergroup complex. In: Johnson MR, Anhaeusser CR, Thomas RJ, editors. The geology of South Africa. Johannesburg: Geological Society of South Africa; 2006. p. 319–24.
37. Eriksson PG, Altermann W, Hartzer FJ. The transvaal supergroup and its precursor complex. In: Johnson MR, Anhaeusser CR, Thomas RJ, editors. The geology of South Africa. Johannesburg: Geological Society of South Africa; 2006. p. 237–60.
38. Cawthorn RB, Eales HV, Walraven F, Uken R, Watkeys MK. The bushveld complex. Geol South Afr. 2006;691:261–82.
39. Skinner EMW, Truswell JF. Kimberlites Complex. The Geology of South Africa. 2006:651–660.
40. Jones CR, Hepworth JV. Geological Map of Botswana. Director of Geological Survey and Mines with the authority of the Ministry of Commerce, Industry and Water Affairs, Gaborone. 1973.